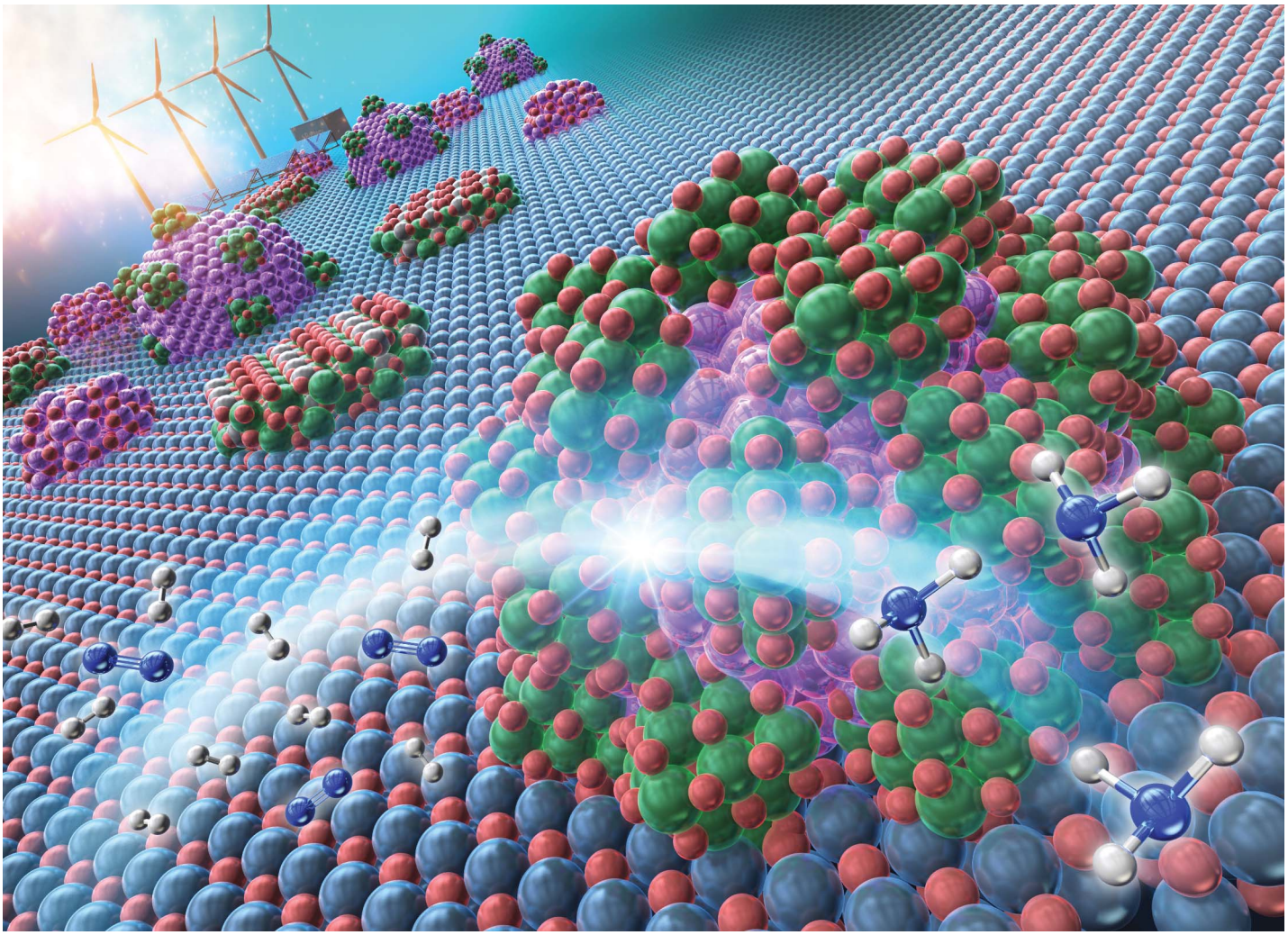

Showcasing research from Professor Katsutoshi Nagaoka's laboratory, Graduate School of Engineering, Nagoya University, Nagoya, Japan.

Barium-doped iron nanoparticles supported on MgO as an efficient catalyst for ammonia synthesis under mild reaction conditions

Encapsulation of Fe nanoparticles by BaO achieves significant ammonia synthesis activity under mild reaction conditions. High temperature reduction induces the accumulation of BaO clusters over Fe nanoparticles. A strong electron donation from this BaO cluster *via* Fe facilitates the cleavage of the dinitrogen triple bond, the rate-determining step in ammonia synthesis. This discovery will contribute to the development of a low-cost ammonia synthesis catalyst that will lead to the realisation of a carbon-neutral society.

As featured in:

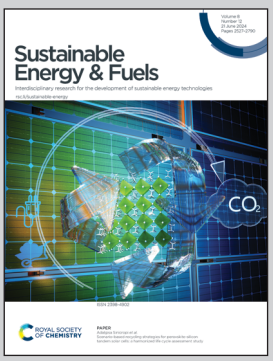

See Katsutoshi Sato, Katsutoshi Nagaoka *et al., Sustainable Energy Fuels,* 2024, **8**, 2593.

ROYAL SOCIETY OF CHEMISTRY

rsc.li/sustainable-energy

Registered charity number: 207890

Sustainable Energy & Fuels

ROYAL SOCIETY OF CHEMISTRY

PAPER

View Article Online
View Journal | View Issue

Cite this: *Sustainable Energy Fuels*, 2024, **8**, 2593

Barium-doped iron nanoparticles supported on MgO as an efficient catalyst for ammonia synthesis under mild reaction conditions†

Kohei Era, [a] Katsutoshi Sato, *[ab] Shin-ichiro Miyahara, [a] Takahiro Naito, [c] Kanishka De Silva, [c] Saeid Akrami, [c] Hiroshi Yamada, [a] Takaaki Toriyama, [d] Takehiro Tamaoka, [d] Tomokazu Yamamoto, [d] Yasukazu Murakami, [de] Koji Inazu [f] and Katsutoshi Nagaoka *[ac]

To realize a carbon-neutral society, developing highly active and inexpensive catalysts for ammonia (NH_3) production working under moderate conditions (<400 °C, <10 MPa) using hydrogen fabricated from the electrolysis of water is demanded. Current industrial fused iron (Fe) catalysts show deficient activity under such conditions. Although Ru-based catalysts have been introduced as highly efficient catalysts working under desired conditions, they are scarce and consequently expensive. This work introduces Fe/Ba/MgO (reduced at 700 °C) as an active catalyst with a high ammonia production rate working at mild temperature and pressure (350 °C, 1.0 MPa). Ba doping to Fe nanoparticles supported on MgO and pre-reduction at high temperatures dramatically ameliorated the NH_3 production rate. Due to the absence of hydrogen poisoning, the catalytic activity of the Fe/Ba/MgO increased gradually by raising the pressure from 0.1 to 3.0 MPa. The activity of this catalyst at 3.0 MPa was higher than that of two benchmark Ru catalysts. After pre-reduction at high temperature, electrons are donated from the BaO encapsulating the Fe^0 nanoparticles to the N_2 molecule, which promotes the rate-determining step of ammonia synthesis. We anticipate that these findings will contribute to developing inexpensive Fe catalysts for decarbonizing the ammonia synthesis process to achieve a carbon-neutral society.

Received 25th March 2024
Accepted 7th May 2024

DOI: 10.1039/d4se00411f

rsc.li/sustainable-energy

Introduction

Ammonia (NH_3) is a promising component for helping to achieve a carbon-neutral society.[1–7] Today, most NH_3 is produced by the industrial Haber–Bosch process using fused Fe-based catalysts. These conventional catalysts, which include Al_2O_3 as a structural promoter and K_2O as a chemical promoter, are introduced as highly active catalysts for NH_3 production at high temperatures of more than 450 °C and pressure higher than 20 MPa.[8] Al_2O_3 and K_2O promoters facilitate the cleavage of the nitrogen bond (N≡N) with a high dissociation energy of 945 kJ mol^{-1}.[8] However, in its current form, the Haber–Bosch process is not suitable for achieving a carbon-neutral society for two reasons. First, the utilized H_2 gas in the process is provided by fossil fuel steam reforming, which leads to the emission of huge amounts of CO_2 (1.9 tons-CO_2 per ton-NH_3).[9] Second, the NH_3 yield of current Fe-based catalysts is significantly decreased at temperatures and pressures lower than 400 °C and 10 MPa, respectively.[10] Thus, novel catalysts are needed that show high NH_3 synthesis activity under mild conditions, which will allow for the use of H_2 produced from clean processes and ultimately, decarbonization of the Haber–Bosch process.[11]

Recently, various alternative NH_3 synthesis catalysts have been developed.[12] Reported Ru catalysts have demonstrated considerable NH_3 yield under moderate conditions, and they are considered the most promising candidates for synthesizing decarbonized NH_3.[13–17] However, Ru utilization in large-scale commercial applications is limited due to its high cost and rarity, and transition elements, such as Mn,[18] Fe,[19] and Co,[20] which are more accessible, have been proposed as catalysts for decarbonized NH_3 synthesis. Fe is the most appropriate element in terms of cost and abundance, which makes the development of Fe-based catalysts for use in a decarbonized NH_3 synthesis process highly desirable.

[a]*Department of Chemical Systems Engineering, Graduate School of Engineering, Nagoya University, Furo-cho, Chikusa-ku, Nagoya, 464-8603, Japan. E-mail: nagaoka.katsutoshi.n2@f.mail.nagoya-u.ac.jp; satou.katsutoshi.j5@f.mail.nagoya-u.ac.jp*

[b]*Institute for Advanced Research, Nagoya University, Furo-cho, Chikusa-ku, Nagoya, 464-8603, Japan*

[c]*Institutes of Innovation for Future Society, Nagoya University, Furo-cho, Chikusa-ku, Nagoya, 464-8603, Japan*

[d]*The Ultramicroscopy Research Center, Kyushu University, Motooka 744, Nishi-ku, Fukuoka, 819-0395, Japan*

[e]*Department of Applied Quantum Physics and Nuclear Engineering, Kyushu University, Motooka 744, Nishi-ku, Fukuoka, 819-0395, Japan*

[f]*National Institute of Technology, Numazu College, 3600 Ooka, Numazu, Shizuoka, 410-8501, Japan*

† Electronic supplementary information (ESI) available. See DOI: https://doi.org/10.1039/d4se00411f

In our previous study, the performance of potassium-doped Fe nanoparticles supported on MgO was investigated for catalytic NH_3 synthesis.[21] Characterization of this catalyst revealed that use of the optimal reduction temperature and the optimal amount of K doping increased the number of Fe^0 nanoparticles on the catalyst surface and the Fe turnover frequency. Moreover, it was reported that a Co/Ba/MgO catalyst prepared by impregnating cobalt(II) acetylacetonate into Ba-doped MgO followed by pre-reduction at high temperature (700 °C) contained BaO encapsulating Co nanoparticles and that this encapsulation dramatically improved the NH_3 synthesis activity of Co.[20] These findings motivated us to study the effects of Ba doping on the catalytic behaviour of the Fe/MgO catalyst.

In this study, the Fe/MgO catalyst doped with barium was employed for the NH_3 synthesis process under mild conditions, and its catalytic behaviour was evaluated. This catalyst showed a high NH_3 production rate (13.8 mmol h^{-1} $g_{cat}{}^{-1}$) under moderate conditions. Moreover, raising the pressure from 1.0 MPa to 3.0 MPa resulted in improving the NH_3 production activity to 26.1 mmol h^{-1} $g_{cat}{}^{-1}$ for the Fe/Ba(1)/MgO-700red (Ba/(Ba + Mg) = 0.01 mol mol^{-1}, pre-reduced at 700 °C) catalyst. This value is more than the activity of two benchmark Ru catalysts (Ru/CeO_2-500red[22] and Cs^+/Ru/MgO-500red[23]). Reduction of Fe/Ba(1)/MgO at 700 °C, a higher temperature than that used for conventional Fe-based catalysts, resulted in the decomposition of $BaCO_3$ and the formation of a structure in which Fe^0 nanoparticles were encapsulated within BaO. This encapsulation led to a significant enhancement of the NH_3 synthesis activity and turnover frequency of Fe/Ba(1)/MgO-700red by electron donation to adsorbed N_2 molecules from the BaO encapsulating Fe^0 nanoparticles. We also discuss the difference in dopant effects between Ba and K.[18]

Experimental

Synthesis of the Ba-doped Fe/MgO catalyst

The stepwise impregnation method was employed to fabricate the Ba-doped Fe/MgO catalyst.[20,21] In this regard, specified amounts of MgO (MgO-500A, Ube Material Industries, Ltd, Japan) and $Ba(OH)_2 \cdot 8H_2O$ (Fujifilm Wako Pure Chemicals, Co., Japan) solution were mixed for 1 h. It should be noted that different amounts of Ba(X) (X = 0.5, 1 and 3) were loaded for investigation of the influence of doping on catalytic behaviour (X is the mole percentage of Ba with respect to the total molar value of Ba plus Mg). After blending, the powder was separated using a rotary evaporator and treated in a muffle furnace at 700 °C for 5 h to form the Ba/MgO support. To deposit the Fe catalyst on the support, iron(III) acetylacetonate [$Fe(acac)_3$] (Tokyo Chemical Industry Co., Ltd, Japan) was mixed with Ba/MgO in tetrahydrofuran (Fujifilm Wako, Japan). The Fe loading amount was considered to be 20 wt% of the catalyst. However, this value was 16.2 wt% according to the X-ray fluorescence analysis after the catalytic tests. The powder and solvent were separated using a rotary evaporator at 35 °C and calcined in a tube furnace in Ar at 500 °C for 5 h. The procedure to synthesize the catalyst without Ba doping (Fe/MgO) was the same as the mentioned route except for the Ba loading step. It should be noted that for this catalyst, MgO was heated in a muffle furnace at 700 °C for 5 h before loading the Fe catalyst.[20] Ru/CeO_2 and Cs^+/Ru/MgO as benchmark catalysts were fabricated utilizing the same method reported before.[20]

Catalytic NH_3 synthesis test

For the catalytic NH_3 synthesis test, 100 mg of catalyst powder was pressed to make a pellet and then was sieved (250–500 μm particle size).[20,21] The pelleted catalyst was located in a tubular Inconel reactor (The Nilaco Corporation, Japan) and reduced at 500 or 700 °C with a 2 °C min^{-1} ramping rate.[20,21] The reduction was performed under a mixture of H_2 and N_2 gas flow for 1 h. The H_2 to N_2 ratio, total stream rate, and pressure were 3, 240 mL min^{-1} and 0.1 MPa, respectively. After reduction, the reactor temperature was decreased under the same flow. Then, the H_2–N_2 stream with H_2/N_2 = 3 and total stream rate of 120 mL min^{-1} was fed to the reactor to obtain the space velocity of 72 000 mL h^{-1} $g_{cat}{}^{-1}$ and the pressure increased to 1.0 or 3.0 MPa. The synthesis rate of the catalysts was measured by trapping the produced NH_3 in 1–10 mM H_2SO_4 solution. The rate decrease in conductivity, measured using an electronic conductivity detector (CM-30R, DKK-TOA, Japan), is employed to calculate the NH_3 synthesis rate based on a standard curve of electronic conductivity (Fig. S1†). All utilized gases in this work were obtained from high-pressure and high-grade (>99.9999%) cylinders and purified using an inline gas purifier (MicroTorr MC50-904FV, SAES Pure Gas, USA).

Kinetic calculations

Kinetic calculations were conducted using a similar procedure reported before at 350 °C and 0.1 MPa.[24–26] Ammonia synthesis reaction rate was calculated using eqn (1) by considering that the synthesis rate of NH_3 depends on the N_2, H_2 and NH_3 pressures. More details regarding the kinetic calculations and retardation index can be found in the ESI.†

$$r = kP_{N_2}{}^{n}P_{H_2}{}^{h}P_{NH_3}{}^{a} \quad (1)$$

Characterization

It should be noted that all catalyst characterizations were performed after samples were passivated with CO_2 (>99.95% purity with O_2 as an impurity).

Scanning transmission electron microscopy (STEM) with high-angle annular dark-field (HAADF) imaging and corresponding Energy dispersive X-ray spectroscopy (EDX) mapping were performed at 120 kV using a JEM-ARM200CF electron microscope (JEOL, Japan). The sample was prepared by crushing the catalysts in ethanol, dispersing them on a carbon-coated copper grid, and drying them at ambient temperature for 1 day in vacuum.

An EDXL 300 apparatus (Rigaku, Japan) was utilized for X-ray fluorescence analysis of the samples.

The crystal structure was examined by X-ray diffraction analysis using a SmartLab X-ray diffractometer (Rigaku) with a CuK_α source. Analysis of X-ray diffraction profiles was conducted using the PDXL2 software (Rigaku) and three databases

(ICDD, COD,[27] AtomWork).[28] The crystallite size of Fe^0 was measured by Scherrer's equation using the Fe^0 (110) peak located at 44.67° in the X-ray diffraction profile.

After pre-treatment under a N_2 flow at 300 °C, the Brunauer–Emmett–Teller method was performed to measure the specific surface area of the catalysts using a BELSORP MINI X-instrument (Micro-Trac BEL, Japan).

The turnover frequencies of Fe/Ba(1)/MgO and Fe/MgO catalysts were determined by CO-chemisorption capacity measurement using a BEL-CAT-II apparatus (Micro-Trac BEL). To prepare the sample, 50 mg of the catalyst was exposed to a mixture flow of H_2 and N_2 (H_2/N_2 = 3, 120 mL min^{-1} total) for reduction. The temperature was increased to 500 or 700 °C with a 2 °C min^{-1} ramping rate and kept constant for 1 h. For pre-treatment, the sample was located under the He flow for 2 h. The temperature decreased to 50 °C, and the sample was flushed with the He flow for 10 min. Pulse chemisorption was utilized for CO-chemisorption measurement under the He flow (30 mL min^{-1}) at 50 °C.

X-ray Absorption Fine Structure (XAFS) analyses of the Fe K-edge were conducted using the BL01B1 beamline at Spring-8 (Hyogo, Japan) with Japan Synchrotron Radiation Research Institute permission. To avoid the natural oxidation of Fe upon exposure to air, the measurements were done using *in situ* XAFS techniques. Samples (50 mg) diluted with boron nitride were pressed into self-supporting disks with 7 mm diameter and located in a quartz *in situ* XAFS cell (Makuhari Rika Glass, Japan). Each disk was reduced by increasing the cell's temperature by 2 °C min^{-1} from room temperature to 500 or 700 °C under a mixed H_2–N_2 gas stream (H_2/N_2 = 3, 120 mL min^{-1} total) and held for 1 h. The spectra were then measured after cooling to 50 °C under the same stream. Measurements of the Fe K-edge were performed in transmission mode using two ion chambers. A Si (111) two-crystal monochromator was used for the monochromatization of X-rays. X-ray energy was calibrated against the spectrum of a standard Fe foil. Data reduction was carried out using the Athena program (ver. 0.9.26) included in the Demeter package.[29]

Infrared spectra of Fe/Ba(1)/MgO measured by *in situ* reduction under a gas flow of H_2–N_2 mixture (H_2/N_2 = 3) were obtained with a spectrometer (FT/IR-6600, JASCO, Japan) equipped with a mercury–cadmium–telluride detector at a resolution of 4 cm^{-1}. The sample (about 10 mg) was pressed into the self-supporting disk (10 mm in diameter), placed in a silica-glass cell with a CaF_2 window, and connected to a closed gas-circulation system (Makuhari). The disk was pre-treated with a H_2–N_2 mixture (H_2/N_2 = 3, about 80 kPa) that had been passed through a liquid N_2 trap and reduced by increasing the temperature of the cell by 10 °C min^{-1} from room temperature to 700 °C. The infrared spectrum of air measured at room temperature was used as the background, and the difference spectrum was obtained by subtracting the background spectrum from the spectrum measured before reduction (fresh) or after reduction at 500 or 700 °C.

Results and discussion

Catalytic NH_3 production

In the first step, the efficiency of the Fe/Ba(1)/MgO catalyst for NH_3 production was evaluated. Since Fe is easily sintered at high temperatures, a low-temperature, slow reduction is generally used.[19,30–32] A previous study on the Fe/K/MgO catalyst indicated that catalyst reduction at 500 °C results in the best NH_3 production rate. However, because Co/Ba/MgO-700red has been previously reported to show high activity, we performed pre-reduction of Fe/Ba(1)/MgO at 700 °C.

Fig. 1 shows the NH_3 synthesis rates and yields *versus* reaction temperature for Fe/Ba(1)/MgO-700red, Fe/Ba(1)/MgO-500red, and Fe/MgO-700red, compared with fused iron (wüstite-based) as the commercial catalyst at 1.0 MPa. It was observed that Fe/Ba(1)/MgO-700red activity was better than that of the other three catalysts at temperatures of 150 °C to 400 °C. As equilibrium NH_3 yields at 350 °C and 400 °C are 14.8 and 7.91%, respectively, NH_3 yields were far below the equilibrium value. Fe/Ba(1)/MgO-700red even showed NH_3 synthesis activity at 150 °C (0.1 mmol h^{-1} g_{cat}^{-1}). From our previous work, it was realized that the K(3)-doped Fe catalyst supported on MgO and reduced at 500 °C cannot produce NH_3 at 150 °C.[21] This indicates that Ba can enhance the NH_3 synthesis activity at lower temperatures. The activity of Fe/Ba (1)/MgO-700red for NH_3 production at 350 °C was 13.8 mmol h^{-1} g_{cat}^{-1}, which is 5.3 times higher than that of Fe/Ba(1)/MgO-500red and Fe/MgO-700red, and 1.6 times higher than that of the commercial catalyst as shown in Table 1. Thus, Ba was found to be an effective additive for Fe nanoparticles, which is similar to what we reported previously for Co nanoparticles.[20] Further analyses revealed that the highest NH_3 synthesis rates were observed for the catalyst with a reduction temperature of 700 °C (Fig. S2†) and when the amount of Ba doping (Ba/(Ba + Mg)) was 0.01 mol mol^{-1} (Fig. S3†).

The catalytic activity for NH_3 production *versus* time at 350 °C and 1.0 MPa was observed in Fig. 2, indicating that the activity of Fe/Ba(1)/MgO-700red slightly decreased at the beginning and then stabilized. At lower amounts of weight hourly space velocity (36 000 mL h^{-1} g_{cat}^{-1}), the NH_3 production activity of the Fe/Ba(1)/MgO-700red catalyst at 350 °C and 1.0 MPa reached 8.8 mmol h^{-1} g_{cat}^{-1}. Even at this lower space velocity, the catalyst synthesized 0.05 mmol h^{-1} g_{cat}^{-1} NH_3 at 150 °C. Fe/

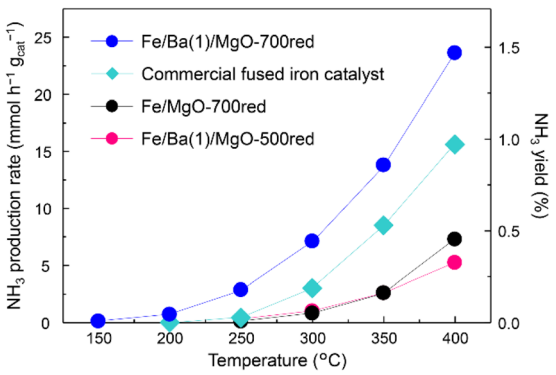

Fig. 1 Ammonia production activity *versus* temperature at 1.0 MPa for Fe/Ba(1)/MgO-700red, Fe/Ba(1)/MgO-500red, Fe/MgO-700red, and a commercial fused iron catalyst. xxxred stands for pre-reduction of the catalyst at xxx °C. Detailed information regarding the commercial catalysts can be found in the ESI.†

Table 1 Properties and ammonia production rate for Fe-based catalysts

Entry	Catalyst	SSA[a] [m^2 g_{cat}^{-1}]	Fe^0 crystallite size[b] [nm]	CO-chemisorption[c] [μmol g_{cat}^{-1}]	Rate[d] [mmol h^{-1} g_{cat}^{-1}]	TOF[e] [s^{-1}]
1	Fe/Ba(1)/MgO-700red	64	10	11.9	13.8	0.322
2	Fe/Ba(1)/MgO-500red	110	7	11.4	2.6	0.063
3	Fe/MgO-700red	90	8	20.5	2.6	0.035
4	Commercial fused iron catalyst	—	—	—	8.6	—

[a] BET specific surface area. [b] Measured by using Scherrer's equation. [c] Measured as CO-chemisorption capacity. [d] Ammonia production rate at 350 °C and 1.0 MPa. [e] Turnover frequency measured from the amount of CO-chemisorption and the ammonia production rate.

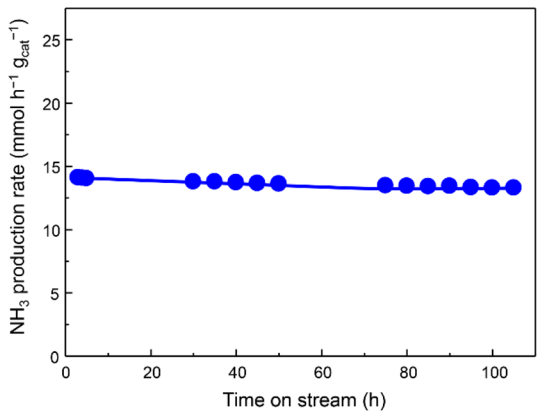

Fig. 2 Ammonia production activity of Fe/Ba(1)/MgO-700red *versus* time course at 350 °C and 1.0 MPa.

Ba(1)/MgO-700red showed NH_3 synthesis activity comparable to Fe-based catalysts, which have been introduced in the literature under mild conditions (Table S1†). Compared to our previously reported Fe/K(3)/MgO-500red, the NH_3 synthesis rate for Fe/Ba(1)/MgO-700red was lower above 300 °C, but it was higher below 250 °C.[21] This suggests that Ba and K have different effects on the NH_3 synthesis activity of Fe^0.

Arrhenius plots of ammonia production reactions using Fe/Ba(1)/MgO-700red, Fe/Ba(1)/MgO-500red, Fe/MgO-700red, and the commercial catalyst are observed in Fig. 3. Following our previous report, the apparent activation energy was calculated separately because the slope changed above and below 300 °C.[21] Here, it was confirmed that these differences were not due to internal diffusion, as the same activity was obtained when testing with smaller catalyst pellets. The different slopes can be attributed to the fact that the adsorbed species which strongly adsorb on the catalyst surface and retard the reaction vary depending on the temperature. Based on the idea that the rate-limiting step is the dissociative adsorption of dinitrogen, this step is retarded by adsorbed species such as NH_x(a) ($x = 0, 1, 2$) and H(a), and these adsorbed species are in equilibrium with gaseous NH_3 and H_2. At lower temperatures, H(a) may be strongly adsorbed on the surface, while at higher temperatures NH_x(a) replaces H(a) as discussed in ref. 33. The apparent activation energies which are equivalent to the slope of the curves were 57.3, 74.5, 111.5, and 85.5 kJ mol^{-1} for Fe/Ba(1)/MgO-700red, Fe/Ba(1)/MgO-500red, Fe/MgO-700red, and the commercial catalyst at temperatures lower than 300 °C, respectively. On the other hand, for the higher temperature range (300–400 °C), it was 38.5, 53.3, 70.5 and 52.5 kJ mol^{-1}, respectively. Thus, Fe/Ba(1)/MgO-700red showed the lowest apparent activation energy over the whole temperature range, suggesting that the high NH_3 synthesis activity of Fe/Ba(1)/MgO-700red resulted from its low apparent activation energy.

The effect of pressure on the NH_3 synthesis activity of Fe/Ba(1)/MgO-700red at 350 °C and also for Cs^+/Ru/MgO-500red and Ru/CeO_2-500red as benchmark Ru catalysts is observed in Fig. 4. Cs^+/Ru/MgO and Ru/CeO_2 are known catalysts due to their activity and for ammonia production by renewable energy utilization, respectively.[22,23] Although the activity of the Fe/Ba(1)/MgO-700red catalyst at 0.1 MPa was lower than that of benchmark Ru catalysts, at 1.0 MPa it was higher than that of Cs^+/Ru/MgO and at 3.0 MPa it improved significantly and reached a value higher than that of both benchmark Ru catalysts.

To determine the reason for the different pressure dependencies of Fe/Ba(1)/MgO-700red and the two benchmark Ru catalysts, we performed kinetic analyses at 350 °C and 0.1 MPa (Table S2 and Fig. S4†). Orders of the reaction with respect to N_2

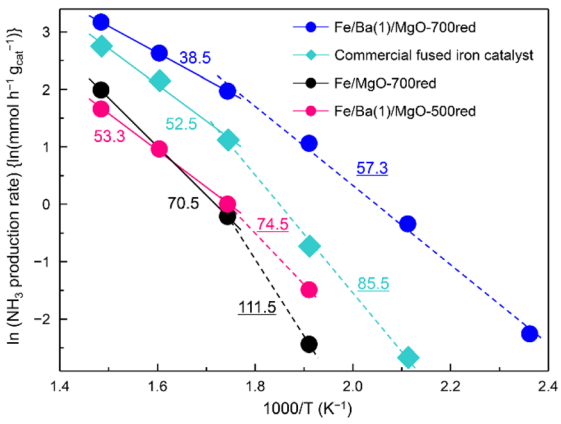

Fig. 3 Arrhenius plots corresponding to ammonia production reactions over Fe/Ba(1)/MgO-700red, Fe/Ba(1)/MgO-500red, Fe/MgO-700red, and a commercial fused iron catalyst at 1.0 MPa. The numbers in the figure denote the apparent activation energy (kJ mol^{-1}) calculated from the slope. The dashed lines and underlined numbers are plots and apparent activation energies below 300 °C, and the solid lines and non-underlined numbers are the plots and apparent activation energies above 300 °C. xxxred stands for pre-reduction of the catalyst at xxx °C.

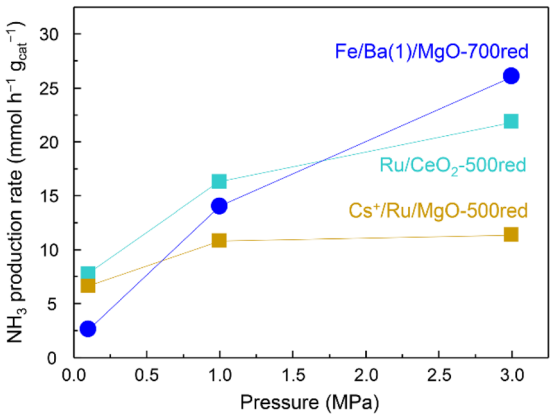

Fig. 4 Ammonia production activity *versus* pressure at 350 °C for Fe/Ba(1)/MgO-700red and two benchmark Ru catalysts. xxxred stands for pre-reduction of the catalyst at xxx °C.

for the three catalysts were almost unity (Table S2†), suggesting that dissociation of N_2 is the rate-determining step. The reaction orders for Cs^+/Ru/MgO-500red and Ru/CeO_2-500red with respect to H_2 were negative. It demonstrates the significant adsorption of hydrogen atoms on the surface of Ru catalysts. This hydrogen adsorption, which is known as hydrogen poisoning, is the main limitation of Ru catalyst utilization. However, the reaction order for Fe/Ba(1)/MgO-700red was positive. Thus, one of the reasons for the increase in NH_3 synthesis rate over Fe/Ba(1)/MgO-700red in response to increased pressure is the absence of hydrogen poisoning. The reaction order for NH_3 was negative for all three catalysts, this value for Fe/Ba(1)/MgO-700red was lower than −1.0, which is a larger negative amount compared to other catalysts. This result shows the significant adsorption of NH_x species on the surface of the catalyst and the equilibrium formed between NH_x and NH_3 components, which prevent N_2 adsorption and activation.

To further investigate the kinetics of Fe/Ba(1)/MgO-700red, the retardation index was considered following previous reports.[21,34] We define the retardation index for NH_x(a) and H(a) as y and z, respectively. A higher value of y indicates strong adsorption of NH_x, while a higher value of z indicates strong adsorption of H. If the sum of y and z exceeds 1 when $x = 0$, then $x = 0$ is not suitable and $x = 1$ or 2 is considered. The calculated retardation index was $(y, z) = (0.69, -0.16)$ when $x = 1$ (Table S3†), meaning that the main surface adsorbed species of Fe/Ba(1)/MgO-700red was NH. The main adsorbed species of Fe/K(3)/MgO-500red estimated in our previous study was N,[21] suggesting that the kinetics and reaction pathways differ, depending on whether K or Ba is doped.

Effect of Ba on the ammonia synthesis activity of Fe/Ba/MgO-700red

The effect of barium doping on the efficiency of the catalysts for NH_3 production, was investigated by evaluating their physicochemical properties. Comparison of these properties for Fe/Ba(1)/MgO-700red, Fe/Ba(1)/MgO-500red, and Fe/MgO-700red is observed in Table 1. Comparison of the catalysts with and without Ba showed that the specific surface area of Fe/Ba(1)/MgO-700red (entry 1) is smaller, and it's Fe^0 crystallite diameter (calculated with Scherrer's equation using the Fe^0 (110) peak in the X-ray diffraction patterns (Fig. S5†)) is larger than that of Fe/MgO-700red (entry 3). For the Fe/Ba(1)/MgO-700red catalyst, the CO-chemisorption capacity, which is considered as an index of Fe dispersion, and the turnover frequency were approximately half and 9.2 times that of Fe/MgO-700red. This means that even though the ratio of surface Fe^0 sites is greater on Fe/MgO-700red than on Fe/Ba(1)/MgO-700red, the latter has significantly more active Fe^0 sites owing to the Ba doping. Here, it was also confirmed that the crystallite size of Fe^0 of Fe/Ba(1)/MgO-700red was 10 nm and was not changed before and after the reaction (Fig. S6†).

Comparison of the Ba-doped catalysts with different reduction treatments showed that Fe/Ba(1)/MgO-700red (entry 1) had about half the specific surface area of Fe/Ba(1)/MgO-500red (entry 2) and a larger Fe^0 crystallite size (Fig. S7†). However, the CO-chemisorption capacity of Fe/Ba(1)/MgO-700red was comparable to that of Fe/Ba(1)/MgO-500red. This is strange from the viewpoint of the sintering of Fe^0 and will be discussed in the section of Effect of Ba on catalyst surface morphology. The turnover frequency of Fe/Ba(1)/MgO-700red was about 5.1 times that of Fe/Ba(1)/MgO-500red, which means that the high-temperature reduction treatment enabled Ba to effectively activate Fe^0.

In the X-ray diffraction pattern of Fe/Ba(1)/MgO-700red, the peaks attributed to $BaCO_3$ that were observed for Fe/Ba(1)/MgO-fresh and Fe/Ba(1)/MgO-500red had disappeared (Fig. S7†). It should be noted that basicity and electron-donating decrease with the formation of carbonates in catalyst samples. Therefore, the significantly improved turnover frequency of Fe/Ba(1)/MgO-700red can be attributed to the decomposition of Ba carbonates during high-temperature reduction. We also performed Fourier transform infrared spectroscopy analyses of Fe/Ba(1)/MgO under an H_2–N_2 mixed gas ($H_2/N_2 = 3$) flow with heating (Fig. S8†). The infrared spectrum of fresh Fe/Ba(1)/MgO before reduction showed characteristic peaks attributed to $MgCO_3$ (1555 cm^{-1}) and $BaCO_3$ (1443 cm^{-1}).[20,35] At 500 °C, the spectrum showed carbonate peaks, but these peaks were primarily absent at 700 °C. Together, these results indicate that higher temperature reduction is necessary to eliminate carbonates from the Ba-doped Fe/MgO catalyst.

Next, we conducted *in situ* X-ray absorption fine structure (XAFS) measurements to investigate the changes induced by Ba doping in the state and local structure of Fe in the catalyst. Fig. 5 shows the Fe K-edge X-ray absorption near edge structure (XANES) spectra of Fe/Ba(1)/MgO and Fe/MgO, as well as spectra of several reference samples. The spectra of the fresh, non-reduced Fe/Ba(1)/MgO (spectrum e) and Fe/MgO (spectrum f) were comparable to that of Fe_3O_4 (spectrum c), suggesting that the valence of Fe in the catalyst was +2 or +3. In the spectra of the reduced samples (spectra g, h, and i), we observed that the intensity of the white line decreased, whereas the intensity of the pre-edge characteristic of the Fe^0 (spectrum a) spectra increased. We examined the degree of reduction of each sample by calculating the fraction of Fe^0 from the linear combination of

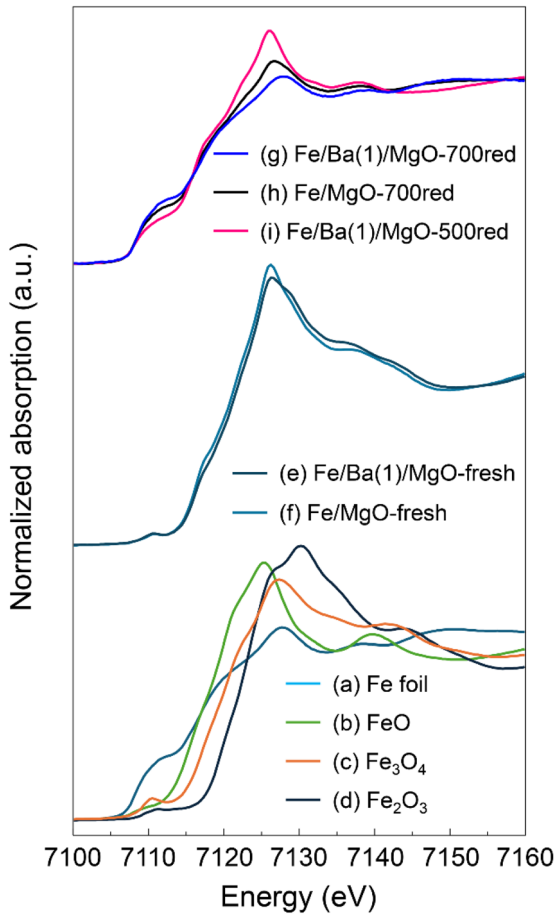

Fig. 5 Normalized Fe K-edge XANES spectra for Fe/Ba(1)/MgO and Fe/MgO before (fresh) and after *in situ* reduction and for reference samples.

the Fe K-edge XANES spectra of FeO and Fe foil. Comparing the catalysts with and without Ba doping, the reduction degree of oxidized Fe species to Fe^0 in Fe/Ba(1)/MgO-700red and Fe/MgO-700red was calculated to be 100% and 85%, respectively; thus, Ba doping enhanced the reduction of oxidized Fe species to Fe^0. Comparing the Ba-doped catalysts with different reduction treatments, the degree of reduction for Fe/Ba(1)/MgO-700red and Fe/Ba(1)/MgO-500red was calculated to be 100% and 54%, respectively, indicating that reduction to Fe^0 is incomplete at 500 °C.

Effect of Ba on catalyst surface morphology

Fig. 6 and S9–S11† show the scanning transmission electron microscopy (STEM) images and corresponding EDX mapping for Fe/Ba(1)/MgO-700red, Fe/Ba(1)/MgO-500red, and Fe/MgO-700red after the catalytic ammonia production experiment as surface morphology evaluation. As shown in our previous report, Fe is oxidized rapidly by trace amounts of oxygen,[21] and because it is challenging to prepare samples completely without exposure to oxygen, the samples were observed after exposed to air using high-magnification, high-angle annular dark-field (HAADF) STEM at atomic resolution. Thus, the contours of the Fe^0 particles were not clear.

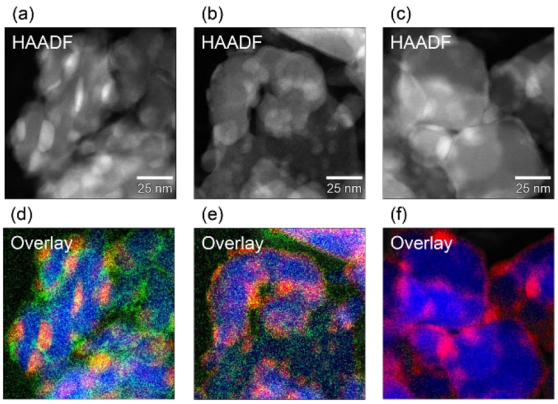

Fig. 6 Comparison of the surface morphology of Fe/Ba(1)/MgO-700red (a and d), Fe/Ba(1)/MgO-500red (b and e), and Fe/MgO-700red (c and f) after the ammonia synthesis test. (a–c) High-angle annular dark-field scanning transmission electron microscopy images. (d–f) Overlay energy dispersive X-ray maps. (d and e) Overlay of Fe K (red), Ba L (green), and Mg K (blue). (f) Overlay of Fe K (red) and Mg K (blue).

EDX mapping for Fe/Ba(1)/MgO-700red after the catalytic ammonia production experiment indicated that Ba was enriched near the Fe^0 particles (Fig. 6a and d). This observation was also reported in our previous work on a barium doped Co catalyst supported on MgO.[20]

Fig. 6 shows the HAADF-STEM images of Fe/Ba(1)/MgO-700red, Fe/Ba(1)/MgO-500red, and Fe/MgO-700red (Fig. 6a–c), and overlay EDX maps of Fe K, Ba L, and Mg K (Fig. 6d and e) and Fe K and Mg K (Fig. 6f). The overlay EDX maps of Fe/Ba(1)/MgO-500red and Fe/MgO-700red indicate that Fe is distributed along the MgO edges. Together with the Fe^0 ratios calculated from the XANES spectra shown in Fig. 5, it can be inferred that the Fe existing along the MgO edges is related to the unreduced Fe oxidized species. In contrast, no such distribution of Fe was observed for Fe/Ba(1)/MgO-700red. This supports our earlier calculation that the fraction of Fe^0 in Fe/Ba(1)/MgO-700red is 100%. Comparison of Fig. 6d and e shows that Ba is enriched near Fe^0 after reduction at 700 °C. This indicates that Fe^0 particles and Ba species move across the MgO surface during reduction at 700 °C, and that the Ba species is enriched in the vicinity of the Fe^0 nanoparticles, reducing the surface energy of Fe^0.[20]

We use our present findings to summarize the influence of reduction temperature on the Fe^0 active sites on a Ba-doped Fe/MgO catalyst. On Fe/Ba(1)/MgO-500red, the degree of reduction to Fe^0 is low, and small Fe^0 nanoparticles are formed. With increased reduction temperature, the Fe oxides on Fe/Ba(1)/MgO-700red are completely reduced, and the size of the Fe^0 nanoparticles is increased. A high reduction temperature leads to decomposition of $BaCO_3$ to $Ba(OH)_2$ with a low melting point, 490 °C, migration of the melted $Ba(OH)_2$ over Fe nanoparticles, decomposition of $Ba(OH)_2$ to BaO, and coagulation of the BaO with a high melting point, resulting in the Fe nanoparticles enriched by BaO nano-fractions.[20] Eventually, the CO-chemisorption of Fe/Ba(1)/MgO-700red is almost the same as that of Fe/Ba(1)/MgO-500red, but the turnover frequency of Fe/Ba(1)/MgO-700red is much higher than that of Fe/Ba(1)/MgO-

500red. The very high turnover frequency of Fe/Ba(1)/MgO-700red can be attributed to the supply of electrons to the antibonding orbital of the nitrogen–nitrogen triple bond from the Fe^0 nanoparticles encapsulated by BaO, which facilitates dissociation of the triple bond.[20]

Finally, we address the different doping effects of Ba and K on Fe nanoparticles in Fe/MgO. Unlike Fe/K(3)/MgO-500red, Fe/Ba(1)/MgO-700red demonstrated ammonia synthesis activity even at a low temperature of 150 °C. This can be attributed to the high N_2 dissociation ability of Fe, which is caused by BaO encapsulation and its enrichment over Fe^0 nanoparticles. K species are volatile and cannot encapsulate Fe^0 nanoparticles, but instead appear to increase the number of Fe^0 on the surface.[21] The main adsorbed species of Fe/Ba(1)/MgO-700red was estimated to be NH at 350 °C, while that of Fe/K(3)/MgO-500red was N.[21] This might be related to the affinity of these catalysts with hydrogen. Such different characteristics of the dopants bring about different behaviours of these catalysts; Fe/Ba(1)/MgO-700red shows higher NH_3 synthesis activity than Fe/K(3)/MgO-500red at low temperatures and *vice versa* at high temperatures.[21]

Conclusions

We report here the catalytic behaviour of Fe/Ba(1)/MgO-700red for NH_3 synthesis under mild reaction conditions. The Fe/Ba(1)/MgO catalyst pre-reduced at 700 °C was about 1.6 times more active per catalyst weight than a commercial fused iron catalyst at 350 °C and 1.0 MPa, and it was able to catalyze the synthesis of NH_3 even at 150 °C. Because Fe/Ba(1)/MgO-700red suffered no hydrogen poisoning, catalyst efficiency improved gradually with raising the pressure from 0.1 to 3.0 MPa, and at 3.0 MPa, the catalyst showed higher activity than two benchmark Ru catalysts. The addition of Ba promoted the reduction of Fe oxides to Fe^0. The reduction of the Fe/Ba(1)/MgO catalyst at 700 °C, a temperature far higher than that used for conventional Fe-based catalysts, caused $BaCO_3$ to decompose and the resulting BaO to be enriched in the vicinity of the Fe^0 nanoparticles. Subsequently, the donation of electrons from BaO encapsulating Fe^0 nanoparticles to the adsorbed N_2 molecules significantly improved the NH_3 synthesis activity and turnover frequency of Fe/Ba(1)/MgO-700red. The dopant effects of K and Ba on Fe nanoparticles are related to their physicochemical properties. Some K is volatile but forms highly dispersed Fe^0 sites, while Ba forms fewer but highly active Fe^0 sites. Furthermore, the main adsorbed species on the catalyst surface were different: NH and N for the Ba-doped and K-doped catalysts, respectively. These differences led to different catalytic behaviours. Our findings are expected to encourage future research on multi-component doping, which promotes the development of inexpensive Fe catalysts to facilitate progress toward a carbon-neutral society.

Author contributions

K. N. designed and he and K. S. coordinated this project. K. E. and S. Miyahara prepared the catalysts, performed the characterizations, and tested catalytic activities. K. E. and K. S. conducted XAFS measurements and analysed the data. T. Toriyama, T. Tamaoka, T. Y. and S. Murakami conducted HAADF-STEM observations and EDX mapping. K. I. performed the catalytic activity tests under high-pressure conditions. All the authors discussed the results and commented on the study. K. E., K.·S., and K. N. co-wrote the manuscript.

Conflicts of interest

There are no conflicts to declare.

Acknowledgements

Part of the results presented in this article was obtained based on a project (JPNP21012) commissioned by the New Energy and Industrial Technology Development Organization (NEDO). STEM-EDX observations were supported by the "Advanced Research Infrastructure for Materials and Nanotechnology in Japan (ARIM)" of the Ministry of Education, Culture, Sports, Science and Technology (MEXT) (Proposal Number JPMXP1223KU0012). K. Sato gratefully acknowledges the financial support from JST FOREST (JPMJFR223N). XAFS measurements were performed at the BL01B1 public beamline of SPring-8 with approval from the Japan Synchrotron Radiation Research Institute (JASRI; proposal no. 2022B1920 and 2023B1679). We thank Mr K. Kato (JASRI) and Dr Y. Nishida (Nagoya Institute of Technology) for their kind support with the XAFS measurements.

References

1 *Ammonia: Zero-Carbon Fertiliser, Fuel and Energy Store*, https://royalsociety.org/topics-policy/projects/low-carbon-energy-programme/green-ammonia/, accessed 19 January, 2024.
2 S. Giddey, S. P. S. Badwal, C. Munnings and M. Dolan, *ACS Sustainable Chem. Eng.*, 2017, **5**, 10231–10239.
3 A. Valera-Medina, H. Xiao, M. Owen-Jones, W. I. F. David and P. J. Bowen, *Prog. Energy Combust. Sci.*, 2018, **69**, 63–102.
4 A. Klerke, C. H. Christensen, J. K. Nørskov and T. Vegge, *J. Mater. Chem.*, 2008, **18**, 2304–2310.
5 K. Eguchi, in *Energy Technology Roadmaps of Japan*, ed. Y. Kato, M. Koyama, Y. Fukushima and T. Nakagaki, Springer Japan, 2016, pp. 167–181, DOI: 10.1007/978-4-431-55951-1.
6 H. Kobayashi, A. Hayakawa, K. D. K. A. Somarathne and E. C. Okafor, *Proc. Combust. Inst.*, 2019, **37**, 109–133.
7 Y. Wang, Y. Tian, S. Y. Pan and S. W. Snyder, *ChemSusChem*, 2022, **15**, e202201290.
8 A. Mittasch and W. Frankenburg, *Adv. Catal.*, 1950, **2**, 81–104.
9 S. L. Foster, S. I. P. Bakovic, R. D. Duda, S. Maheshwari, R. D. Milton, S. D. Minteer, M. J. Janik, J. N. Renner and L. F. Greenlee, *Nat. Catal.*, 2018, **1**, 490–500.
10 K. Sato and K. Nagaoka, *Chem. Lett.*, 2021, **50**, 687–696.
11 D. R. MacFarlane, P. V. Cherepanov, J. Choi, B. H. R. Suryanto, R. Y. Hodgetts, J. M. Bakker,

F. M. Ferrero Vallana and A. N. Simonov, *Joule*, 2020, **4**, 1186–1205.
12 H. Liu, *Chin. J. Catal.*, 2014, **35**, 1619–1640.
13 N. Saadatjou, A. Jafari and S. Sahebdelfar, *Chem. Eng. Commun.*, 2014, **202**, 420–448.
14 K.-i. Aika, *Catal. Today*, 2017, **286**, 14–20.
15 M. Hattori, S. Iijima, T. Nakao, H. Hosono and M. Hara, *Nat. Commun.*, 2020, **11**, 2001.
16 M. Kitano, Y. Inoue, M. Sasase, K. Kishida, Y. Kobayashi, K. Nishiyama, T. Tada, S. Kawamura, T. Yokoyama, M. Hara and H. Hosono, *Angew. Chem., Int. Ed.*, 2018, **57**, 2648–2652.
17 K. Sato, S.-i. Miyahara, Y. Ogura, K. Tsujimaru, Y. Wada, T. Toriyama, T. Yamamoto, S. Matsumura and K. Nagaoka, *ACS Sustainable Chem. Eng.*, 2020, **8**, 2726–2734.
18 P. Wang, F. Chang, W. Gao, J. Guo, G. Wu, T. He and P. Chen, *Nat. Chem.*, 2017, **9**, 64–70.
19 W. Al Maksoud, R. K. Rai, N. Morlanés, M. Harb, R. Ahmad, S. Ould-Chikh, D. Anjum, M. N. Hedhili, B. E. Al-Sabban, K. Albahily, L. Cavallo and J.-M. Basset, *J. Catal.*, 2021, **394**, 353–365.
20 K. Sato, S.-i. Miyahara, K. Tsujimaru, Y. Wada, T. Toriyama, T. Yamamoto, S. Matsumura, K. Inazu, H. Mohri, T. Iwasa, T. Taketsugu and K. Nagaoka, *ACS Catal.*, 2021, **11**, 13050–13061.
21 K. Era, K. Sato, S. I. Miyahara, T. Naito, K. De Silva, S. Akrami, H. Yamada, T. Toriyama, T. Yamamoto, Y. Murakami, K. I. Aika, K. Inazu and K. Nagaoka, *ChemSusChem*, 2023, **16**, e202300942.
22 T. Nanba, Y. Nagata, K. Kobayashi, R. Javaid, R. Atsumi, M. Nishi, T. Mochizuki, Y. Manaka, H. Kojima, T. Tsujimura, H. Matsumoto, T. Fujimoto, K. Suzuki, T. Oouchi, S. Kameda, Y. Hoshino, S. Fujimoto, M. Kai and Y. Fujimura, *J. Jpn. Petrol. Inst.*, 2021, **64**, 1–9.
23 R. Javaid, H. Matsumoto and T. Nanba, *ChemistrySelect*, 2019, **4**, 2218–2224.
24 K. Aika, J. Kubota, Y. Kadowaki, Y. Niwa and Y. Izumi, *Appl. Surf. Sci.*, 1997, **121–122**, 488–491.
25 R. Kojima and K.-i. Aika, *Appl. Catal., A*, 2001, **219**, 157–170.
26 K. Imamura, S.-i. Miyahara, Y. Kawano, K. Sato, Y. Nakasaka and K. Nagaoka, *J. Taiwan Inst. Chem. Eng.*, 2019, **105**, 50–56.
27 S. Grazulis, D. Chateigner, R. T. Downs, A. F. Yokochi, M. Quiros, L. Lutterotti, E. Manakova, J. Butkus, P. Moeck and A. Le Bail, *J. Appl. Crystallogr.*, 2009, **42**, 726–729.
28 Y. Xu, M. Yamazaki and P. Villars, *Jpn. J. Appl. Phys.*, 2011, **50**, 11RH02.
29 B. Ravel, M. Newville and J. Synchrotron, *Radiat.*, 2005, **12**, 537–541.
30 H. Fan, X. Huang, K. Kahler, J. Folke, F. Girgsdies, D. Teschner, Y. Ding, K. Hermann, R. Schlogl and E. Frei, *ACS Sustainable Chem. Eng.*, 2017, **5**, 10900–10909.
31 P. Q. Yan, W. H. Guo, Z. B. Liang, W. Meng, Z. Yin, S. W. Li, M. Z. Li, M. T. Zhang, J. Yan, D. Q. Xiao, R. Q. Zou and D. Ma, *Nano Res.*, 2019, **12**, 2341–2347.
32 M. Hattori, N. Okuyama, H. Kurosawa and M. Hara, *J. Am. Chem. Soc.*, 2023, **145**, 7888–7897.
33 C. M. Goodwin, P. Lomker, D. Degerman, B. Davies, M. Shipilin, F. Garcia-Martinez, S. Koroidov, J. Katja Mathiesen, R. Rameshan, G. L. S. Rodrigues, C. Schlueter, P. Amann and A. Nilsson, *Nature*, 2024, **625**, 282–286.
34 K. Aika, M. Kumasaka, T. Oma, O. Kato, H. Matsuda, N. Watanabe, K. Yamazaki, A. Ozaki and T. Onishi, *Appl. Catal.*, 1986, **28**, 57–68.
35 E. Roedel, A. Urakawa, S. Kureti and A. Baiker, *Phys. Chem. Chem. Phys.*, 2008, **10**, 6190–6198.

